Kent Academic Repository

Mao, Chun-Xu, Khalily, Mohsen, Xiao, Pei, Brown, Tim W. and Gao, Steven (2019) *Planar Sub-Millimeter-Wave Array Antenna with Enhanced Gain and Reduced Sidelobes for 5G Broadcast Applications.* IEEE Transactions on Antennas and Propagation, 67 (1). pp. 160-168. ISSN 0018-926X.

Planar Sub-Millimeter-Wave Array Antenna with Enhanced Gain and Reduced Sidelobes for 5G Broadcast Applications

Chun-Xu Mao, *Member, IEEE,* Mohsen Khalily, *Senior Member, IEEE*, Pei Xiao, *Senior Member, IEEE*, Tim W. C. Brown, *Member, IEEE*, Steven Gao, *Senior Member, IEEE*

Abstract—In this paper, a compact, broadband, planar array antenna with omnidirectional radiation in horizontal plane is proposed for the 26 GHz fifth-generation (5G) broadcast applications. The antenna element is composed of two dipoles and a substrate integrated cavity (SIC) as the power splitter. The two dipoles are placed side-by-side at both sides of the SIC and they are compensated with each other to form an omni-directional pattern in horizontal plane. By properly combing the resonant frequencies of the dipoles and the SIC, a wide impedance bandwidth from 24 to 29.5 GHz is achieved. To realize a large array while reducing the complexity, loss and size of the feeding network, a novel dual-port structure combined with radiation and power splitting functions is proposed for the 1st time. The amplitude and phase on each element of the array can be tuned, and therefore, the grating lobes level can be significantly reduced. Based on the dual-port structure, an 8-element array with an enhanced gain of over 12 dBi is designed and prototyped. The proposed antenna also features low profile, low weight and low cost, which is desirable for 5G commercial applications. Measured results agree well with the simulations, showing that the proposed high-gain array antenna has a broad bandwidth, omni-directional pattern in horizontal plane, and low side-lobes.

Index Terms—Antenna, Array, broadband, broadcast, millimeter-wave (mm-Wave), omni-directional, fifth-generation (5G).

I. INTRODUCTION

THE development of the wireless communication systems has been significantly changing our life styles in the past two decades. To support the potential wireless applications, such as multimedia devices, Internet of things (IoT), intelligent transportation system (ITS), an advanced mobile system with a gigabit per second data rate is highly desired, which cannot be handled by current fourth-generation (4G) communication

Fig. 1. Aston soccer stadium for 5G broadcast test spot.

systems due to the limited bandwidth. To overcome the bandwidth limitation, the International Telecommunication Union (ITU) has licensed several millimeter-wave (mm-Wave) spectrums for the potential 5G and beyond applications, including 24.25-27.5 GHz, 37-40 GHz and 66-76 GHz [1]. Since then, much attention has been paid to the research of mm-Wave antennas, in both academia and industry.

To realize the gigabit data rate while overcoming the high loss in high frequency bands, several promising techniques, including high-gain array antennas and multibeam antennas (MBAs), are likely to be adopted in the 5G communication systems [2]-[4]. Recently, array antennas with broad bandwidths and high gains were investigated based on planar waveguides [5]-[6], substrate integrated waveguides (SIWs) [7]-[8], and microstrip techniques [9]-[11]. In [12]-[14], a variety of MBAs were achieved based on reflectarrays [12], transmission lenses [13], and beamforming circuits [14]. The combination of mm-Wave antennas with MIMO technology within a compact size were also investigated for both base-stations [15] and mobile terminals [16]. Besides, the mm-Wave antennas with dual- or multi-band operations were reported [17]-[18].

Although a few mm-Wave antennas have been proposed for the 5G wireless applications, they are facing the problems such as bulky structure, installation difficulty, high steering loss, and high cost. In many circumstances where many potential users are evenly distributed in a spacious area, such as auditoriums, stadiums, shopping malls and working offices, the antenna with omnidirectional radiation in horizontal plane but narrow beam in vertical plane is preferred for saving radiating power. Because conventional omni-directional antennas in horizontal plane, such as monopole and dipole, have a low gain
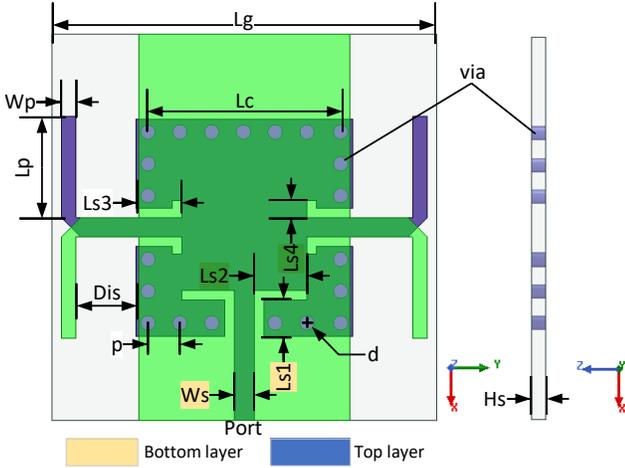
Fig. 2. Configuration of the proposed omni-directional antenna element. Lg = 8 mm, Lc = 4 mm, Lp = 2.1 mm, Wp = 0.3 mm, Dis = 1.6 mm, p = 0.66 mm, d = 0.3mm, Ws = 0.4 mm, $Ls1$ = 0.95 mm, $Ls2$ = 1.1 mm, $Ls3$ = 0.95 mm, $Ls4$ = 0.4 mm.

(2-4 dBi), an array antenna with multiple elements along vertical orientation is required to enhance the gain in horizontal plane. To the best of the authors' knowledge, very few mm-wave array antennas with the omni-directional radiation pattern in horizontal plane have ever been reported. In [19], a circular polarization omni-directional antenna element is proposed for 5G applications. But it suffers from limited bandwidth (27-28.5 GHz) and complex geometry.

In this paper, a compact high-gain planar array antenna with omni-directional radiation in horizontal plane is proposed for the 5G broadcast applications. As a proof-of-concept, an array antenna is designed to cover the Aston Stadium in Birmingham, as shown in Fig. 1. The antenna can also be used in other scenarios. The novelty of this antenna includes: (1) a new method of realizing the omnidirectional radiation pattern in horizontal plane by employing two side-by-side dipoles; (2) substrate integrated cavity (SIC) is adopted in the antenna design to realize the power divider and also the resonant structure for enhancing the impedance bandwidth; (3) more importantly, a novel dual-port multi-functional structure which combines the functions of power dividing and radiation is investigated for realizing a large array. Compared with other reported works, the proposed antenna also features low cost, low profile, and low side-lobe.

This paper is organized as follow. Section II discusses the design principles, including SIC-based antenna element, dual-port radiation/transmission unit, and subarray. Section III presents the proposed 8-element array antenna. Section IV summaries the experimental and measurement results and followed by Conclusion.

II. ANTENNA ELEMENT AND SUBARRAY DESIGN

In this part, the design principles and considerations of the targeted broadband omni-directional antenna element and its evolution processes are firstly illustrated. Then, a novel dual-port module is presented, which combines the functions of
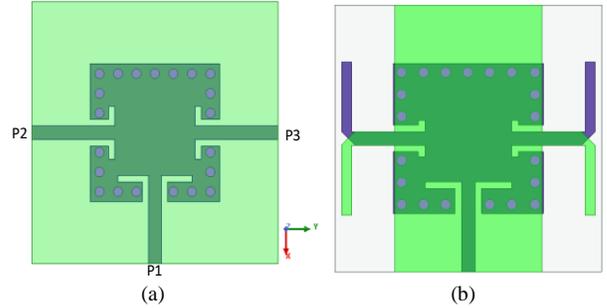

Fig. 3. Configurations of the SIC-based structures: (a) two-way power splitter, (b) proposed dual-dipole antenna.

the radiation and power splitting to form an initial 2-element subarray.

A. Broadband Omnidirectional Dual-Dipole Element

For a 5G antenna working at a high frequency band up to 26 GHz, a broad impedance bandwidth is basically required. Fig. 2 shows the configuration of the proposed broadband antenna element, which consists of two side-by-side dipoles and a substrate integrated cavity (SIC) between them. The SIC serves as a two-way power splitter, which splits the input power evenly between the two dipoles. The square cavity is realized by connecting the top and bottom metallic layers with a circle metallic via holes. A grounded coplanar waveguide (CPWG) is used as the transformer between the microstrip line and the SIC [20]. The dominant resonant frequency of the SIC can be derived by using the substrate integrated waveguide (SIW) methods [21],

$$f_o = \frac{c}{2\sqrt{\varepsilon_r}} \sqrt{\left(\frac{1}{L_{eff}}\right)^2 + \left(\frac{1}{W_{eff}}\right)^2} \tag{1}$$

where L_{eff} and W_{eff} are the effective length and width of the cavity, ε_r is the relative dielectric constant of the substrate. Here, due to $L_{eff} = W_{eff}$ in this design, the equation (1) can be simplified as,

$$f_0 = \frac{c}{L_{eff}} \sqrt{\frac{1}{2\varepsilon_r}} \tag{2}$$

where

$$L_{eff} = L_c - \frac{d^2}{0.95\,p} \tag{3}$$

where d is the diameter of the via-hole, p is the space between two via holes. Here, the resonant frequencies of the SIC and dipoles are synchronically tuned to form the 2nd-order resonant circuit, which is beneficial to improving the impedance bandwidth [22]-[23]. This will be detailed in the following sections.

B. Evolution

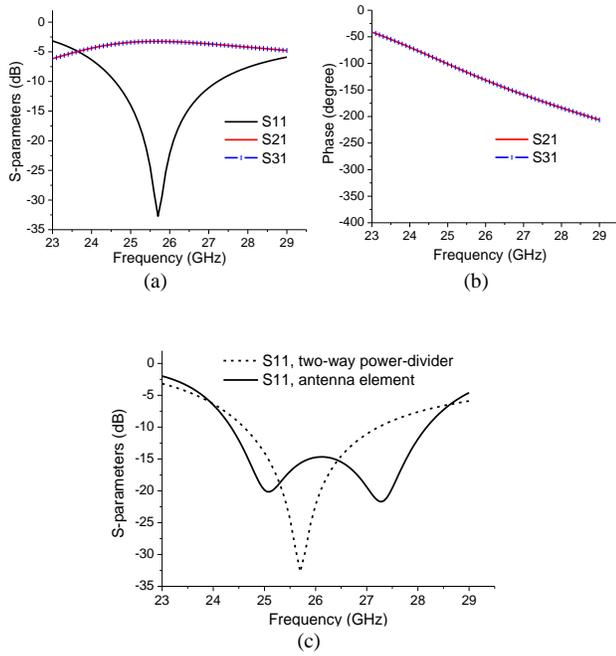The proposed horizontal plane omni-directional antenna is

Fig. 4. Simulated S-parameters of the SIC-based power splitter and the proposed antenna element: (a) amplitudes of the power splitter, (b) phases of the power splitter, (c) S_{11} comparison between the power splitter and the antenna element in Fig. 3.

Fig. 5. Simulated S_{11} with different parameters changed: (a) length of the grounded CPWG, L_{s1}; (b) length of the grounded CPWG, L_{s2}; (c) distance between the dipole and the SIC, Dis; (d) length of the dipole, L_p.

developed from a SIC-based two-way power splitter, as the configuration shown in Fig. 3(a). For comparison, the proposed antenna element is also shown in Fig. 3(b). The SIC-based power splitter is composed of a SIC and three microstrip lines as the outputs. The grounded CPWG is used to transform the microstrip to the SIC. Here, P1 is the input, while P2 and P3 are the two in-phase outputs. Because the splitter is symmetrical along the x-axis, the input power can be evenly split between the two outputs. The operating frequency of the cavity is determined by the dimension of the cavity, which can be evaluated using the equation (2). Compared with the power splitter, the antenna element is realized by cutting off the ground of the two outputs and extending two arms from the ground plane of the cavity. The length of each arm is about a quarter guided wavelength of the center frequency, 26 GHz.

Fig. 4 shows the simulated amplitude and phase properties of the S-parameters of the power splitter. As can be observed from Fig. 4(a), the center frequency of the power splitter is designed at 25.8 GHz and a -15dB bandwidth from 25 to 26.8 GHz is achieved. The curve lines of the S_{21} and S_{31} are overlapped with each other over the entire frequency band, indicating the input power can be evenly split between the two outputs (two dipoles for the antenna). Around the center frequency, $|S_{21}|$ and $|S_{31}|$ is about 3.2 dB, indicating a very low insertion loss of 0.2 dB, even at mm-Wave frequency band. Viewing the results in Fig. 4(b), we can see a similar phenomenon that the two outputs have the same phase characteristics.

To further enhance the impedance bandwidth, the counterpart antenna is achieved by conceiving a direct coupling between the dipoles and the SIC. This results in the 2nd-order resonant characteristics at the input and therefore an improved impedance bandwidth with two reflection zeros can be
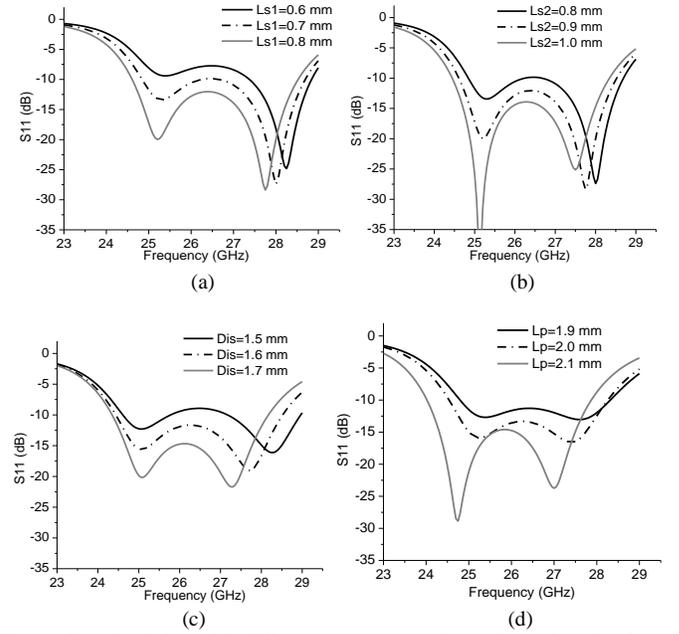
identified at 25 and 27.2 GHz, as shown in Fig. 4(c). Compared with the power splitter, the -15dB impedance bandwidth of the antenna is improved from 6.9% to 13.5%. In addition, due to the antenna is developed from a balanced power splitter, a balanced radiation at the two dipoles can be achieved.

The impedance matching performance of the antenna is mainly influenced by the grounded coplanar waveguide transformers between the SIC, the microstrip line, and the radiating dipoles. To illustrate it, parametric studies are carried out and shown in Fig. 5. Fig. 5(a) and (b) show that the S_{11} of the antenna is improved as the lengths of the grounded CPWG increase, denoted as L_{s1} and L_{s2} in Fig. 2. Besides, the distance between the dipole and the cavity (denoted as Dis) and the length of the dipoles (denoted as L_p) also have an evident effect on the matching performance of the antenna, as shown in Fig. 5(c) and (d). It should be noted that the values of the Dis and L_p can directly lead to the change of the dipole's resonant frequency. When the resonant frequencies of the SIC and dipoles are matched well, very good impedance matching performance can be achieved.

Fig. 6(a) shows the simulated current distribution of the antenna element at 26 GHz. It is observed that the current is distributed evenly on the two dipoles. For each dipole, the currents on the two arms have the same orientation, generating the omnidirectional radiation pattern in the yz-plane. However, due to the obstruction of the metallic SIC, the pattern in the opposite direction of the dipole is suppressed. This uneven radiation can be compensated by employing two side-by-side dipoles located both sides of the cavity. In this way, the influence of the feeding networks on the radiation can be eliminated and a good omnidirectional radiation pattern in the H-plane is realized, as shown in Fig. 6(b). In the E-plane (xz-plane), a dumbbell-like radiation pattern is achieved.
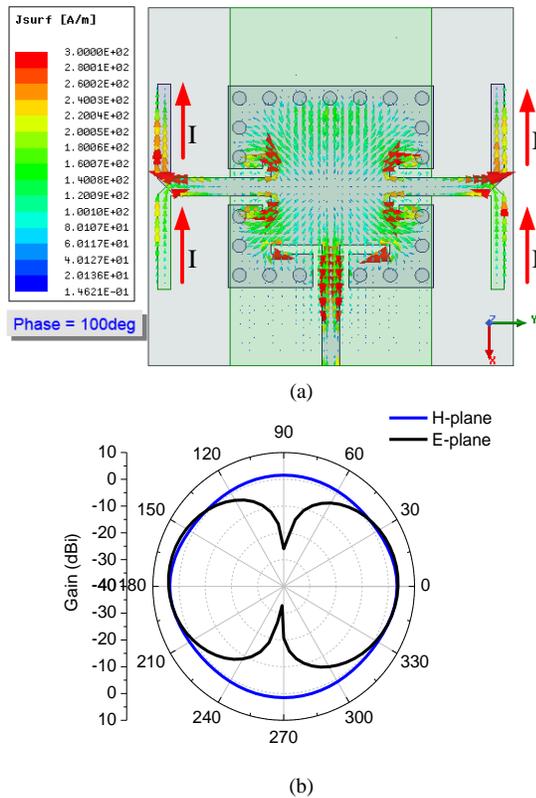
(a)

(b)

Fig. 6. (a) Simulated current distribution on the antenna element at 26 GHz; (b) simulated E- and H-plane radiation patters of the antenna.
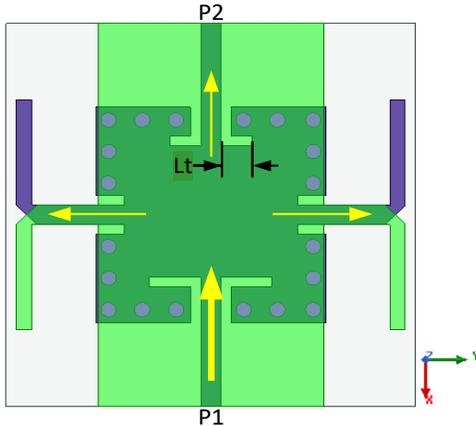

Fig. 7. Configuration of the proposed dual-port radiation/transmission unit.

C. Dual-Port Radiation/Transmission Module

To realize a large array antenna, a conventional large multi-way power splitter is required [24]. This is usually a very challenging task for the omni-directional antenna array antenna, since a large feeding network will block the radiation in some directions, especially at mm-Wave frequencies, where the feed is electrically large. To overcome this problem, a novel dual-port compact module, which combines the functions of radiating and power splitting simultaneously, is proposed, as shown in Fig. 7. This multifunctional module is developed from the element in Fig. 2 with an additional output (P2) on the opposite side of input. The input power from the P1 is partly
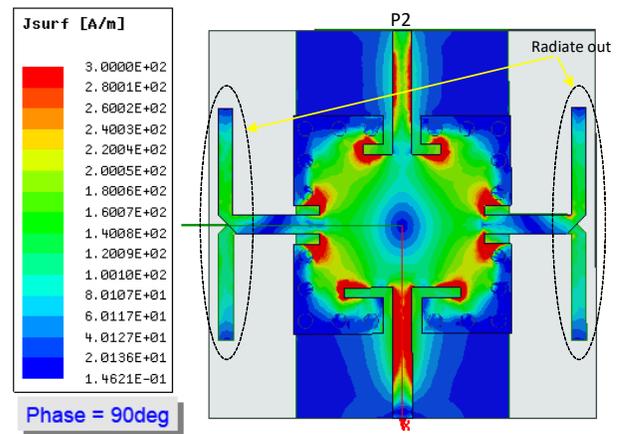

Fig. 8. Simulated current distribution of the proposed dual-port radiation/transmission unit.
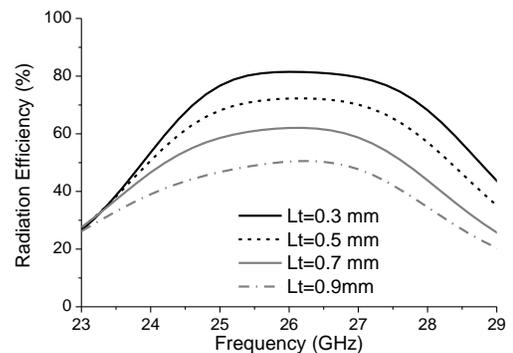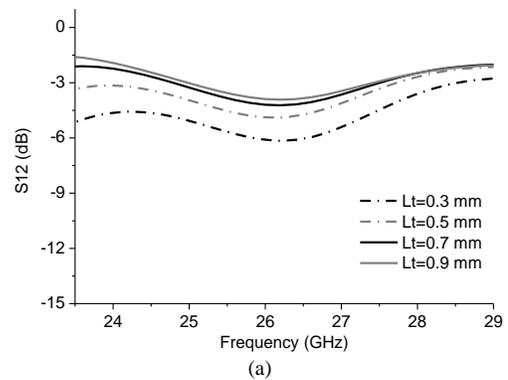

(a)

Fig. 9. Simulated S_{21} and radiation power of the dual-port unit with different Lt: (a) S_{21}, (b) radiation power.

transmitted to the two dipoles for radiation, and the rest power is transmitted through the SIC and output from P2. This dual-port radiation/transmission module can handle the radiation and power splitting without increasing the complexity of the design. To illustrate it, the current distribution of the dual-port module at 26 GHz is shown in Fig. 8. As can be seen, a part of the input power is evenly radiated out via the two dipoles. The rest of the power is output from the P2, which can be served as the input of another antenna element. Also, we can observe that the current intensity at the output is noticeably reduced as compared with the current at the input.

Since the dual-port unit combines the functions of radiation and transmission of the input power, it is important to

TABLE I
DISTRIBUTION OF THE TRANSMITION COEFFICIENT TO
RADIATION EFFICIENCY DEPENDENT ON CPWG LENGTH

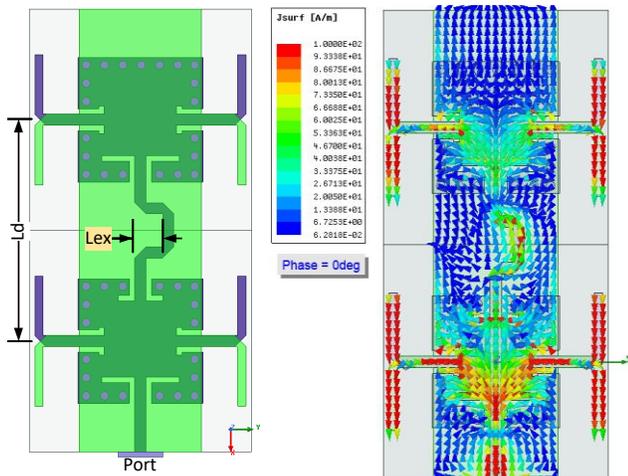| L_t (mm)	Radiation efficiency (%)	Transmission coefficient (%)	Total efficiency (%)
0.1	79%	19.5%	98.5%
0.2	74%	23.2%	97.2%
0.3	70%	28.5%	98.5%
0.4	65%	32.6%	97.6%
0.5	59%	39.6%	98.6%
0.6	53%	44.3%	97.3%
0.7	49%	47.2%	96.2%
0.8	44%	50.1%	94.1%
0.9	39%	53.3%	92.3%
1	35%	56.6%	91.6%

Fig. 10. (a) Configuration of the 1 × 2 subarray, (b) Simulated current distribution of the subarray at 26 GHz. L_d = 8 mm, L_{ex} = 1 mm.

Fig. 11. Simulated radiation patters of the 1 × 2 subarray at 26 GHz: (a) E-plane, and (b) H-plane.

understand how to control the proportion of the power for radiating out and the power for transmitting at the output. To illustrate it, a parametric study has been carried out, which shows that the length of the grounded CPWG between the cavity and P2 has a significant influence on the power distribution, denoted as L_t in Fig. 7. Fig. 9(a) shows the simulated S_{21} of the dual-port module with different L_t. The results show that the power transmitted from the P1 to the P2 increases as L_t increases from 0.3 mm to 0.9 mm. Correspondingly, the power radiating out from the dipoles is reduced from 80% to 45%. Thus, the proportion of the radiation power and transmission power can be easily controlled by adjusting the length of L_t. This fact is very useful in the array antenna design, which will be detailed in the following parts.

To support the array antenna design in the next section, the proportion of the radiation power, transmission power and the total efficiency of the dual-port module variation with different L_t is extracted through the HFSS full-wave simulation and summarized in Table-I. As L_t increases from 0.1 mm to 1 mm, the proportion of the radiation power decreases from 79% to 35%. In contrast, the proportion of transmission between the two ports is increased from 19.5% to 56.6%. The total
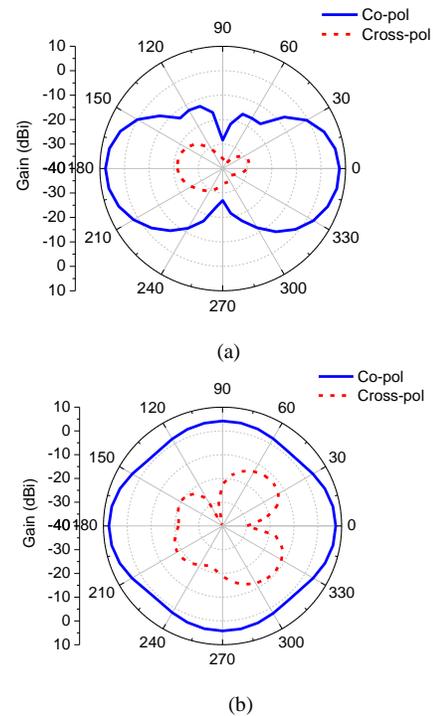
efficiency, which combines the radiation portion and transmission portion, is maintained over 90% when L_t is changed from 0.1 to 1 mm, showing that the proposed dual-port module has a high efficiency.

D. Subarray

Based on the studies of the antenna element and the dual-port module, a 1 × 2 subarray operating at 26 GHz is first investigated by simply connecting them using a microstrip, as shown in Fig. 10(a). The distance between the two elements, L_d, is set as 8 mm, which is around 0.7 wavelengths at 26 GHz. A meandered microstrip line is used to connect the output of the radiation/transmission module with the input of the other antenna element. The length of the microstrip line is used to control the phase delay between the two elements and thus in-phase radiation characteristics can be achieved.

Fig. 10(b) shows the simulated current distribution on the subarray at 26 GHz. It is observed that the antenna has the in-phase current distribution on the two sets of dipoles, which results in an enhanced directivity in the far-field. Moreover, the strength of the current on the two elements are almost identical, which is realized by adjusting the length of L_t, as indicated in Table I. Since traditional two-way power splitting networks and impedance transformers are not needed in this design, the size and complexity of the subarray are significantly reduced. Moreover, because the microstrip transmission line is placed between the radiation elements, the blockage of the feeding networks on the radiation pattern can be avoided. It should be noted that there are some current flowing along both edges of the copper plane outside the cavity, which is mainly induced by the radiating dipoles on both sides.

Fig. 11 shows the simulated co- and cross-polarization radiation patterns in E and H-plane, respectively. It is observed
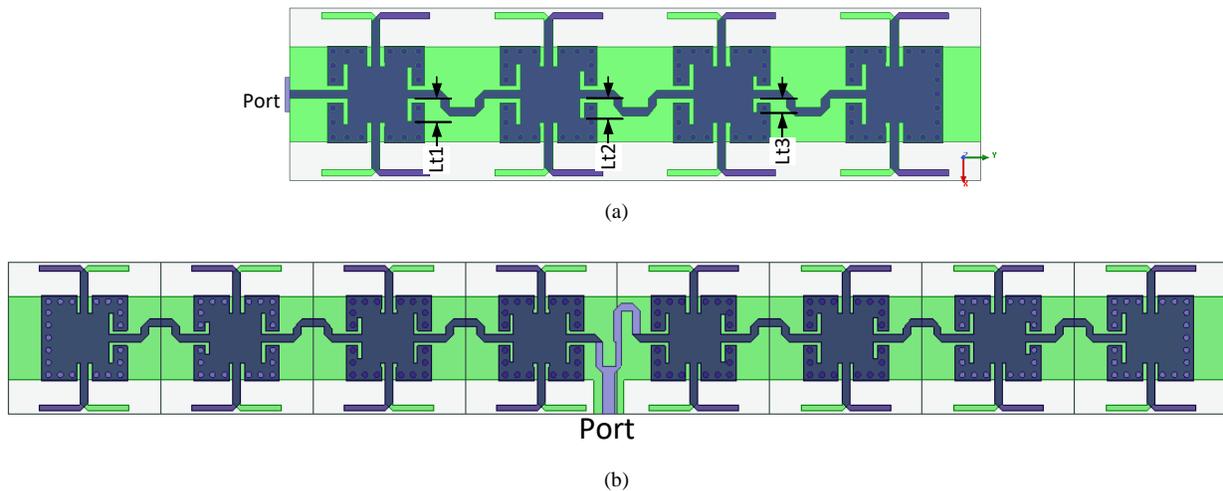
(a)

(b)

Fig. 12. Configurations of the proposed antenna arrays: (a) 1×4 subarray, (b) 1×8 array. $Lt1 = 0.9$ mm, $Lt2 = 0.7$ mm, $Lt3 = 0.5$ mm.
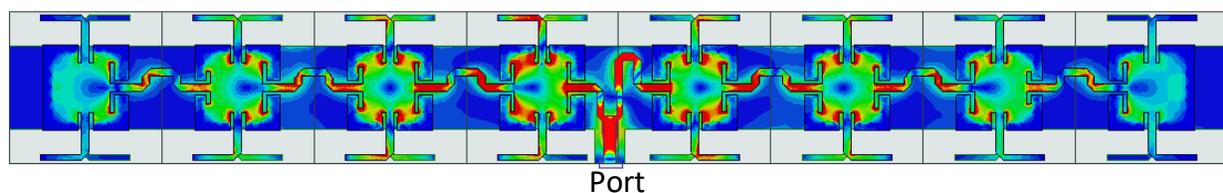

Fig. 13. Simulated current distribution of the proposed antenna arrays at 26 GHz.

that the subarray exhibits a good omni-directional radiation performance in the H-plane (*yz*-plane). In the E-plane (*xz*-plane), the antenna exhibits a dumbbell-like radiation pattern with a gain of 7 dBi. Besides, the antenna exhibits a very low cross polarization discrimination (XPD).

III. HIGH-GAIN OMNI-DIRECTIONAL ARRAY ANTENNA

To enhance the gain, a 1×8 array antenna is conceived based on the elements and subarrays proposed, as shown in Fig. 12(b). The 1×8 array is composed of two 1×4 subarrays, which is shown in Fig. 12(a). For each 1×4 subarray, four antenna elements are connected in series without incurring bulky feeding networks. To produce a good radiation performance with a low sidelobe, it is crucial to control the power distribution on each element. Traditionally, a gradient power distribution on the elements of an array could effectively suppress the unwanted sidelobes. By using the HFSS full-wave simulation, the proportion of the power on the four elements is set as 4: 2.5: 1.5: 1. Looking up the Table-I, the lengths of the transformers, denoted as L_{t1}, L_{t2} and L_{t3}, are chosen as $L_{t1} = 0.9$ mm, $L_{t2} = 0.7$ mm, $L_{t3} = 0.5$ mm, respectively.

It should be noted that the 1×8 array is conceived by mirroring the 1×4 subarray along the symmetrical axis and connected using an out-of-phase two-way power splitter. Therefore, the proportions of the radiation power on the elements (from the left to the right) are 1: 1.5: 2.5: 4: 4: 2.5: 1.5: 1. Fig. 13 shows the current distribution of the proposed 1×8 array at the center frequency 26 GHz. It is observed that the current intensity is gradient from the central part to the two ends of the array antenna.

IV. RESULTS AND DISCUSSION

The proposed 1×8 array antenna was prototyped and shown in Fig. 14. To facilitate the soldering with an mm-Wave connector, the antenna is slightly enlarged, and the overall size of the prototype is 66 mm × 15 mm × 0.3mm. Simulation results shows that this change has no evident influence on the antenna performance. Fig. 15 shows the simulated and measured S-parameters of the array antenna. Both results agree reasonably well with each other, showing a broad impedance bandwidth from 24 to over 29 GHz. The minor discrimination between the simulation and measurement is caused by the fabrication tolerance and the influence of the high-frequency connector.

Fig. 16 shows the simulated and measured antenna gains of the proposed 1×8 array antenna. The measured results agree well with the simulations over a broadband. The antenna has a flat gain of over 10 dBi from 24.8 to 27.7 GHz. In the frequency band of interest, the average measured gain is around 11.5 dBi, which is about 1 dB below the simulations. This is attributed to the insertion losses of the connectors and cables. The gain gradually decreases beyond the band, which is mainly caused by the deformation of the radiation pattern and impedance mismatching. The simulated radiation efficiency is over 90% in the band of interest. Due to the limitation of measurement, the measured radiation efficiency is not provided.

Fig. 17 shows the simulated and measured normalized radiation patterns of the proposed array antenna at 26 GHz. The measured results agree well with the simulations, showing the quasi omni-directional radiation pattern in the horizontal plane
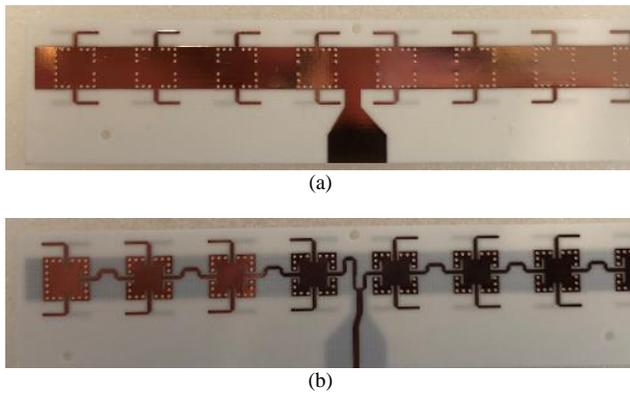
(a)

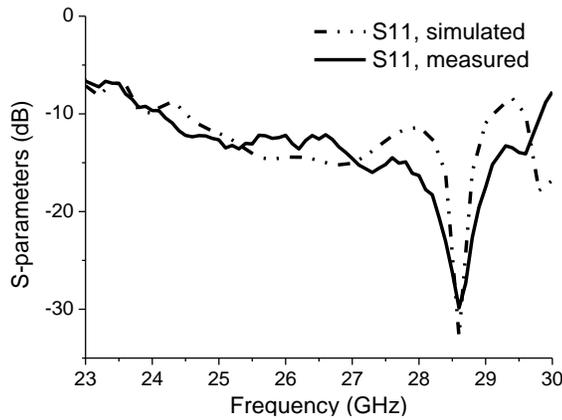Fig. 14. Prototype of the proposed 1×8 array antenna: (a) back view, (b) front view.

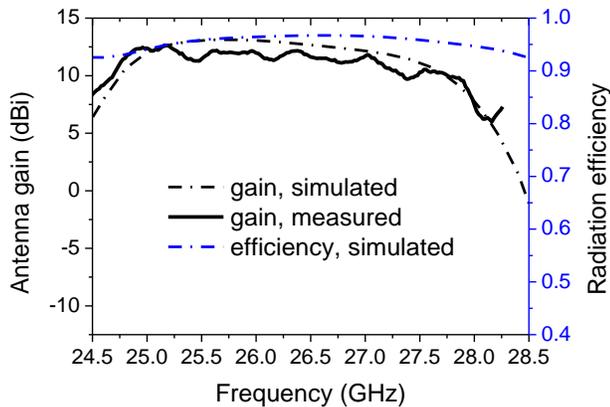Fig. 15. Simulated and measured S-parameters of the 1×8 array.

Fig. 16. Simulated and measured antenna gain and radiation efficiency.

(a)

(b)

(c)

Fig. 17. Simulated and measured normalized radiation patterns of the array antenna at 26 GHz, (a) yz-plane, (b) xy-plane, and (c) xz-plane.

(*yz*-plane). In the E-plane (*xy*-plane and *xz*-plane), the antenna exhibits the maximum radiation in the horizontal plane. The measured 3-dB beam-width is 13.3° and the sidelobes are lower than -15 dB. The measured XPD in main beams direction is over 20 dB.

V. CONCLUSION

In this paper, a compact linear sub-millimeter-wave array antenna with enhanced gain and omni-directional radiation is proposed for 5G broadcast applications. The proposed antenna is realized by usin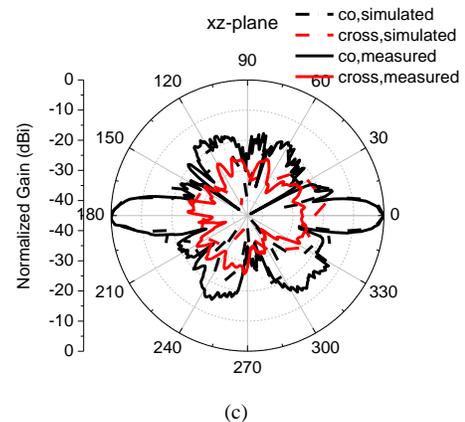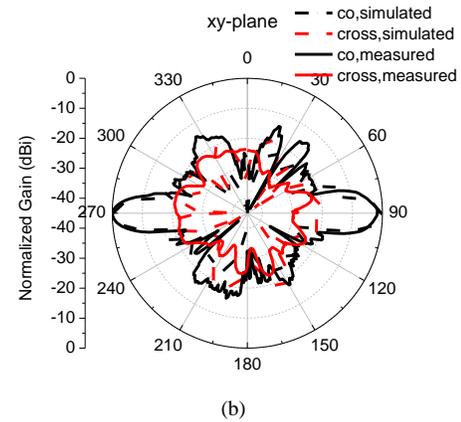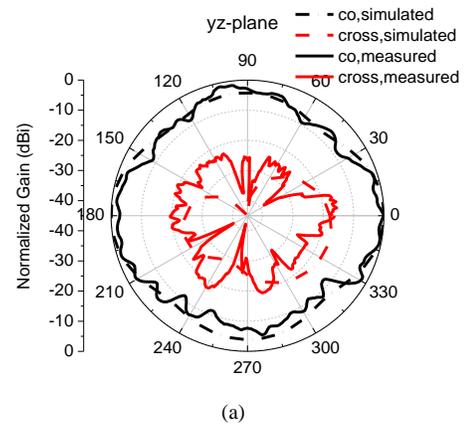g two side-by-side dipoles and a SIC-based power splitting network between them. Omni-directional radiation in horizontal plane is achieved over a broad bandwidth thanks to the integrated design of dual-dipole and SIC. In addition, a novel multi-functional module which combines the functions of radiation and transmission is put forward and studied carefully. The methods of controlling the proportion of radiating power and transmission power are investigated for the 1st time. To validate the concept, an 8-element array antenna with the gain of over 11 dBi is realized without resorting a large feeding network. Such a compact, low-profile, planar antenna could significantly reduce the manufacturing and installation cost in the potential 5G applications. The antenna is prototyped and tested and measured results agree well with the simulations.

REFERENCES

[1] M. J. Marcus, "5G and 'IMT for 2020 and beyond' [spectrum policy and regulatory issues]," *IEEE Wireless Commun.*, vol. 22, no. 4, pp. 2–3, Aug. 2015.

[2] W. Hong *et al.*, "Multibeam antenna technologies for 5G wireless communications," *IEEE Trans. Antennas and Propag.*, vol. 65, no. 12, pp. 6231-6249, Dec. 2017.

[3] T. Rappaport *et al.*, "Millimeter wave mobile communications for 5G cellular: It will work!" *IEEE Access*, vol. 1, pp. 335-349, 2013.

[4] M. H. Dahri, M. H. Jamaluddin, M. I. Abbasi and M. R. Kamarudin, "A review of wideband reflectarray antennas for 5G communication systems," *IEEE Access*, vol. 5, pp. 17803–17815, 2017.

[5] J. Guo, S. Liao, Q. Xue and S. Xiao, "Planar aperture antenna with high gain and high aperture efficiency for 60-GHz applications," *IEEE Trans. Antennas and Propag.*, vol. 65, no. 12, pp. 6262-6273, Dec. 2017.

[6] M. H. Dahri, M. H. Janaluddin, M. Khalily, M. I. Abbasi, R. Selvaraju, M. R. Kamarudin, "Polarization diversity and adaptive beamsteering for 5G reflectarrays: A Review," *IEEE Access*, vol. 6, pp. 19451-19464, 2018.

[7] Q. Zhu, K. B. Ng, C. H. Chan and K. M. Luk, "Substrate-integrated-waveguide-fed array antenna covering 57–71 GHz band for 5G applications," *IEEE Trans. Antennas and Propag.*, vol. 65, no. 12, pp. 6298-6306, Dec. 2017.

[8] J. W. Lian, Y. L. Ban, Q. L. Yang, B. Fu, Z. F. Yu, and L. K. Sun, "Planar millimeter-wave 2-D beam-scanning multibeam array antenna fed by compact SIW beam-forming network," *IEEE Trans. Antennas and Propag.*, vol. 66, no. 3, pp. 1299-1310, Mar. 2018.

[9] C. X. Mao, S. Gao and Y. Wang, "Broadband High-Gain Beam-Scanning Antenna Array for Millimeter-Wave Applications" *IEEE Trans. Antennas and Propag.*, vol. 65, no. 9, pp. 4864-4868, Sep. 2017.

[10] Y. Gao, R. Ma, Y. Wang, Q. Zhang and C. Parini, "Stacked patch antenna with dual-polarization and low mutual coupling for massive MIMO," *IEEE Trans. Antennas and Propag.*, vol. 64, no. 10, pp. 4544-4549, Oct. 2016.

[11] M. Khalily, R. Tafazolli, P. Xiao and A. Kishk, "Broadband mm-Wave Microstrip Array Antenna with Improved Radiation Characteristics for Different 5G Applications," *IEEE Trans. Antennas and Propag.*, vol. 66, no. 10, pp. 4641-4647, Sept. 2018.

[12] R. R. Romanofsky, "Advances in scanning reflectarray antennas based on ferroelectric thin-film phase shifters for deep-space communications," *Proc. IEEE*, vol. 95, no. 10, pp. 1968–1975, Oct. 2007.

[13] Y. J. Cheng *et al.*, "Substrate integrated waveguide (SIW) Rotman Lens and its Ka-band multibeam array antenna applications," *IEEE Trans. Antennas and Propag.*, vol. 56, no. 8, pp. 2504-2513, Aug. 2008.

[14] P. Chen *et al.*, "A multibeam antenna based on substrate integrated waveguide technology for MIMO wireless communications," *IEEE Trans. Antennas Propag.*, vol. 57, no. 6, pp. 1813–1821, Jun. 2009.

[15] B. Yang, Z. Yu, Y. Dong, J. Zhou and W. Hong, "Compact tapered slot antenna array for 5G millimeter-wave massive MIMO systems," *IEEE Trans. Antennas and Propag.*, vol. 65, no. 12, pp. 6721-6727, Dec. 2017.

[16] N. Ojaroudiparchin, M. Shen, S. Zhang and G. F. Pedersen, "A switchable 3-D-coverage-phased array antenna package for 5G mobile terminals," *IEEE Antennas Wireless Propag. Lett.*, vol. 15, pp. 1747–1750, 2016.

[17] W. Zhai, V. Miraftab, M. Repeta, D. Wessel, W. Tong, "Dual-band millimeter-wave interleaved antenna array exploiting low-cost PCB technology for high speed 5G communication," *in Proc. IEEE MTT-S International Microwave Symposium (IMS)*, pp. 1-4, 2016.

[18] S. F. Jilani, A. Alomainy, "A multiband millimeter-wave 2-D array based on enhanced Franklin Antenna for 5G wireless systems," *IEEE Antennas Wireless Propag. Lett.*, vol. 16, pp. 2983–2986, 2017.

[19] W. Lin and R. Ziolkowski, "Compact, omni-directional, circularly-polarized mm-Wave antenna for device-to-device (D2D) communications in future 5G cellular systems," *in Proc. 10th Global Symposium on Millimeter-Waves*, pp. 115-116, 2017.

[20] X. P. Chen and K. Wu, "Low-loss ultra-wideband transition between conductor-backed coplanar waveguide and substrate integrated waveguide," in *IEEE MTT-S Int. Microw. Symp. Dig.*, pp. 349–352, Jun. 2009.

[21] X. P. Chen K. Wu, "Substrate integrated waveguide filter with improved stopband performance for satellite ground terminal," *IEEE Trans. Microw. Theory Techn.,* vol. 57, no. 3, pp. 674-683, Mar. 2009.

[22] C. X. Mao, S. Gao, Y. Wang, F. Qin and Q. X. Chu, "Multi-mode resonator-fed dual polarized antenna array with enhanced bandwidth and selectivity," *IEEE Trans. Antennas and Propag.*, vol. 63, no. 12, pp. 5492-5499, Dec. 2015.

[23] C. X. Mao, *et al.*, "Dual-band filtering-antenna with controllable bandwidth and harmonics suppression," *IEEE Trans. Antennas and Propag.*, vol. 64, no. 9, pp. 4074-4077, Sep. 2016.

[24] C. Mao, S. Gao, Q. Luo, T. Rommel and Q. Chu, "Low-cost X/Ku/Ka-band dual-polarized array with shared aperture," *IEEE Trans. Antennas and Propag.*, vol. 65, no. 7, pp. 3520-3527, Jul. 2017.